Hindawi
Geofluids
Volume 2022, Article ID 3209790, 12 pages
https://doi.org/10.1155/2022/3209790

Research Article

Main Controlling Factors and Formation Mode of Geothermal Anomaly in Eastern Chenghe Mining Area of Weibei Coalfield

Tao Peng,[1,2] **Kaixiang Liu**,[3] **Yue Chen**,[1,2] **Feng Wang**,[4] **and Bing Li**[5]

[1]*College of Geology and Environment, Xi'an University of Science and Technology, Xi'an 710054, China*
[2]*Key Laboratory of Coal Resources Exploration and Comprehensive Utilization, Ministry of Natural Resources, Xi'an 710021, China*
[3]*China Coal Xi'an Design Engineering Co., Ltd., Xi'an 710054, China*
[4]*Shaanxi Coal Chenghe Mining Co., Ltd., Chengcheng 715200, China*
[5]*Shaanxi 139 Coal Geology & Hydrogeology Co., Ltd., Weinan 714000, China*

Correspondence should be addressed to Tao Peng; pengtao@xust.edu.cn

Received 13 June 2022; Revised 20 August 2022; Accepted 23 August 2022; Published 7 September 2022

Academic Editor: Liang Xin

Geothermal anomaly has gradually become a prominent issue affecting the efficient mining of coal with the depth of coal mining increasing in eastern Chenghe mining area of Weibei coalfield. Here, we comprehensively investigated the distribution characteristics of the present geothermal field, analyzed the main controlling factors, and constructed forming mode of geothermal anomaly by the temperature measurement in surface borehole and underground water, combined with coal-rock thermal conductivity test. The results show that the geothermal gradient ranged from 25.7°C/km to 54.3°C/km. The areas with geothermal gradient greater than 30°C/km accounted for 88.31%, and there was the highest gradient value in the southeast F_1 fault zone. The heat flow was between 66.81 mW/m^2 to 128.49 mW/m^2, which belonged to the obvious high heat flow area. Under the action of the main controlling factors such as fault, fold, coal-rock thermal conductivity, and groundwater activity in the region, the geothermal gradient and geothermal heat flow values showed an increasing trend from northwest to southeast. According to the distribution characteristics of heat flow and the action mechanism of main controlling factors, the geothermal anomaly in the study area was finally divided into two forming modes, i.e., fault-deep circulating hot water uplifting type and coal seam heat resistance-fold type. The research provides guidance for the geothermal hazard prevention of coal mine and the rational development and utilization of geothermal resources.

1. Introduction

Geothermal energy has been gaining more and more attention in the past decade due to the huge amounts of geothermal resources and their wide distribution, as well as its environmentally friendly advantages [1–3]. However, it must be noted that high geothermal hazard in coal mine has become a new problem following roof collapse, gas explosion, fire hazard, water inrush, and coal dust with the increase of mining depth [4–11]. Hence, the distribution characteristics and controlling factors of geothermal anomaly are important research contents of mine geothermal hazard prevention and comprehensive development of geothermal resources [12–17].

In general, the geothermal gradient is higher in the eastern basins and lower in the western basins in China. The geothermal resource abundance is also higher in eastern and the Beibuwan basin in China, and the geothermal source forming condition is better, followed by the Ordos, Qaidam, and Sichuan basins [18]. Many scholars have conducted studies on the geothermal field and thermal evolution history of the Ordos Basin and made a series of important progress in the current geothermal field, geothermal evolution history, thermal events, and other aspects of the basin

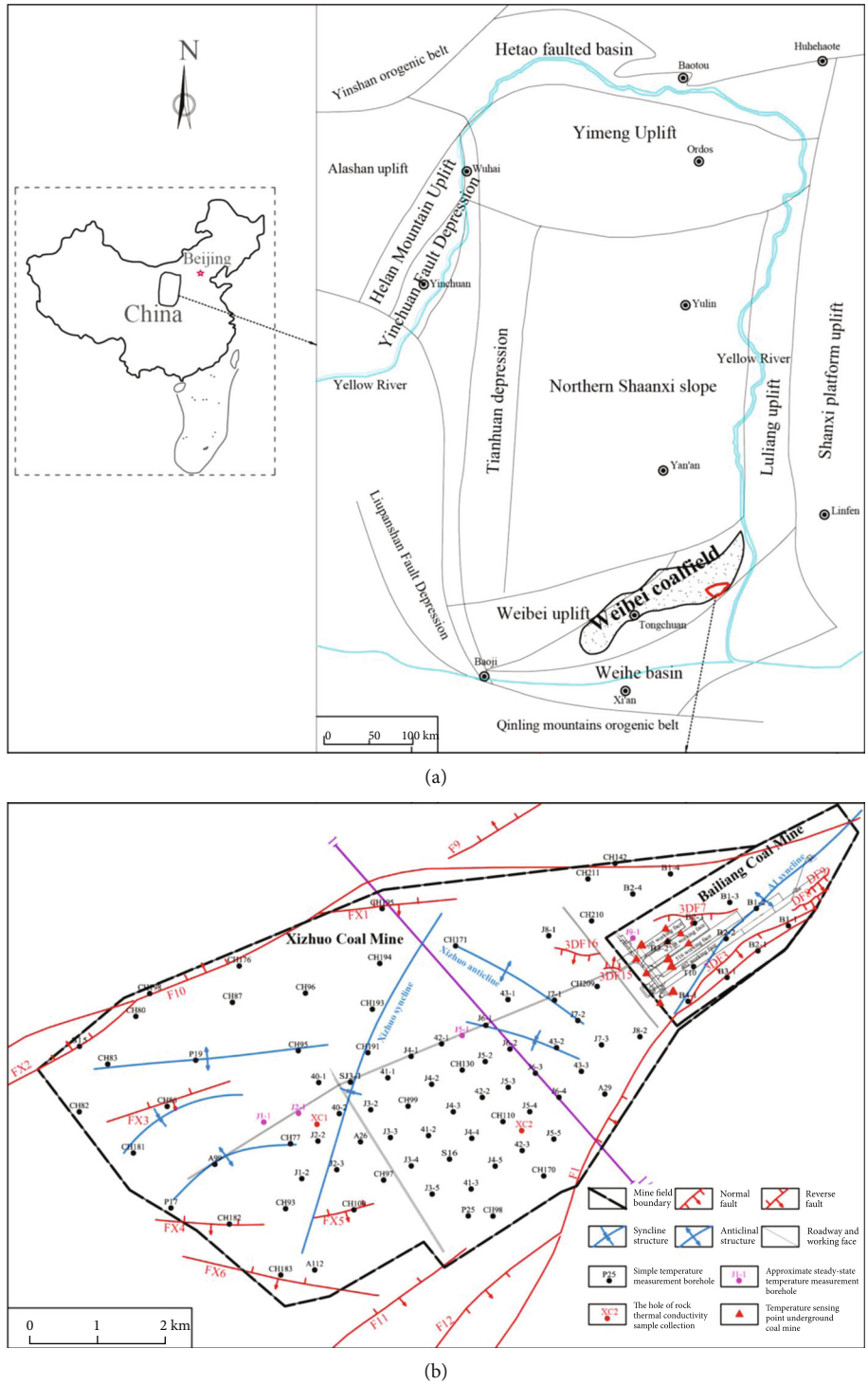

Figure 1: Structure outline and temperature measurement point distribution of the study area ((a) structural outline of Ordos Basin; (b) study area structure outline).

[19–25]. Geothermal anomalies are the result of a combination of geological factors, groundwater, tectonics, faults, and thermal evolution all affect geothermal distribution and heat flow [26–32]. Geothermal sources, channels, reservoirs, and caps constitute the entire geothermal system. Jolie et al. [33] considered that the main driver of geothermal activity is elevated crustal heat flow, which is focused in regions of active magmatism and/or crustal thinning. Permeable structures such as faults exercise a primary control on local fluid flow patterns, with most upflow zones residing in complex fault interaction zones. Uzelli et al. [34] found that Varto and the surrounding region have important geothermal fields, developing in strike-slip tectonic setting in East Anatolia, which resulted from the collision of the Arabian and

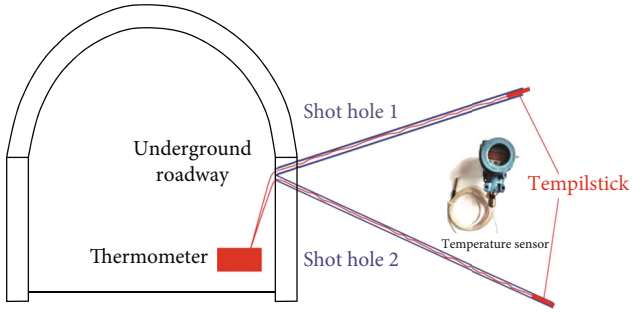

Figure 2: Schematic diagram of temperature measurement arrangement.

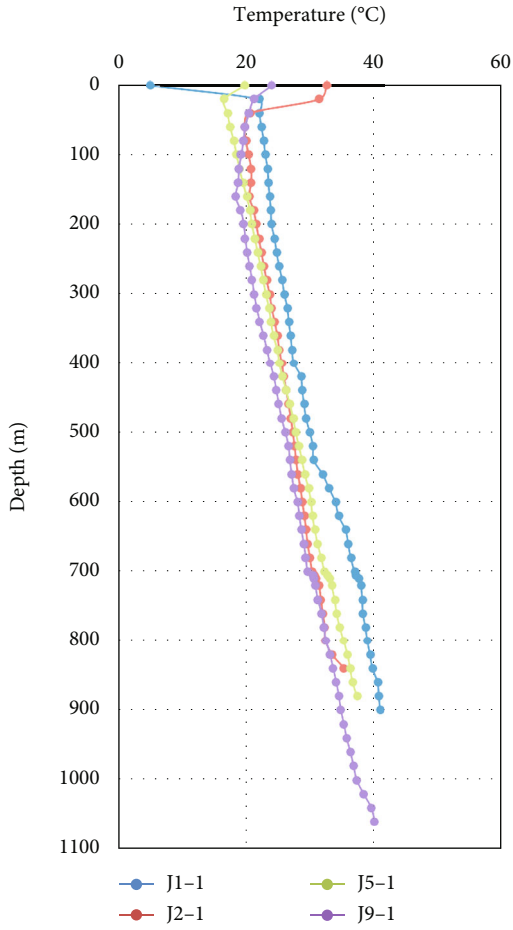

Figure 3: Typical well temperature logging curve.

Eurasian plates. The planes of strike-slip faults in transtensional areas are more favorable for secondary permeability and enhances the geothermal fluid circulation. Guo et al. [35] show that thermal conductivity differences among Cenozoic caprock, Proterozoic carbonate reservoirs, and basement rock mainly affect the geothermal distribution in the Xiong'an New Area. Convective type is a common geothermal system [36, 37]. Groundwater rises to geothermal reservoirs through heat-controlling faults, causing convective heat transfer and increasing the geothermal reservoir temperature. Therefore, high-temperature groundwater accumulates in the shallow uplift areas.

Weibei Carboniferous-Permian coalfield located in the southeastern margin of Ordos Basin is an important coal mining base in China. According to the results of geothermal survey in coal mining areas, the potential risk of thermal hazard is relatively small in northwest coal mining areas [38–40]. But Xizhuo and Bailiang mine, located in Chenghe mining area of Weibei coalfield, have appeared relatively rare phenomenon of mine thermal hazard. When the mining depth is more than 400 m, the air temperature of underground working face is more than 32°C, and the water inrush temperature of mine floor is more than 40°C. Geothermal hazard in mines seriously restrict the safe and efficient mining of coal resources in this area. At present, no special research work on mine geothermal has been carried out in Weibei coalfield, and there is a lack of comparative study on various geological conditions affecting mine geothermal field. Therefore, the distribution characteristics of geothermal and the causes of geothermal anomalies need to be further studied.

In this context, the current geothermal field distribution characteristics and geothermal differences were carried out a detailed analysis based on the borehole temperature logging data and the test of coal-rock thermal conductivity. Second, the spatial variation of geothermal transfer conditions was further studied, and main controlling factors of geothermal field were revealed. Finally, according to the distribution characteristics of heat flow and the action mechanism of main controlling factors, and the formation mode of geothermal anomaly was constructed. It provided scientific basis for geothermal hazard prevention and geothermal resources.

2. Geological Settings

2.1. Geological Structure. The study area is Xizhuo mine and Bailiang mine in the east of Chenghe mining area in Weibei coalfield. Due to the influence of regional tectonic setting and large fault at the edge of the mining area, the strata in the eastern part of Chenghe mining area are monocline strike NEE and dip NNW, accompanied by a series of secondary folds and secondary fault, with a relatively gentle dip angle, generally less than 15°.

The southern boundary of the study area is the regional F_1 Hancheng large fault belt, which strikes NE and dip SE with a dip angle of 70° and a maximum drop of 550 m. The northern boundary is the regional F_{10} fault belt, which strikes NEE, dip WNN, and dip angle 70°. The drop of F_{10} fault belt from west to east gradually increases to 420 m, and it intersects with F_1 fault in the northeast of the study area. According to the actual exposure of the two mines, there are also a number of normal faults of small size in the area, with a drop of less than 15 m in general (Figure 1).

2.2. Strata and Coal Seam. The strata in the area are, respectively, from old to new: Middle Ordovician Fengfeng group (O_2f), Upper Carboniferous Taiyuan group (C_3t), Lower Permian Shanxi group (P_1s), Lower Permian Xiashihezi group (P_1sh), Upper Permian Shangshihezi group (P_2sh), Upper Permian Sunjiagou group (P_2s), Lower Triassic Liujiagou

Table 1: Statistics of thermal conductivity of rock samples.

Hole number	Depth/m	Serial number	Lithology	Thermal conductivity W/m·°C
XC1	136-138	XC1-1	Fine sandstone	2.41
	178-181	XC1-2	Medium sandstone	2.72
	338-340	XC1-3	Sandy mudstone	2.89
	345-347	XC1-4	Coarse sandstone	3.60
	493-496	XC1-5	Sandy mudstone	4.14
	509-511	XC1-6	Siltstone	4.59
	524-525	XC1-7	Fine sandstone	3.43
	558-570	XC1-8	Mudstone	2.63
	571-579	XC1-9	Fine sandstone	4.12
	587	XC1-10	Mudstone	3.06
	604	XC1-11	Sandy mudstone	5.07
XC2	127-130	XC2-1	Sandstone	4.12
	145-148	XC2-2	Sandy mudstone	2.24
	154-157	XC2-3	Fine sandstone	3.98
	162-163	XC2-4	Mudstone	2.79
	280-290	XC2-5	Sandy mudstone	3.75
	334-340	XC2-6	Medium sandstone	3.99
	406-409	XC2-7	Fine sandstone	2.24
	415-418	XC2-8	Medium sandstone	3.98
	421-424	XC2-9	Mudstone	2.79
	436-439	XC2-10	Fine sandstone	3.29
	442-444	XC2-11	Mudstone	2.56
	465-470	XC2-12	Mudstone	1.95
	455-456	XC2-13	Mudstone	3.71
	473-475	XC2-14	Mudstone	2.99

group (T_1l), Lower Triassic Heshanggou group (T_1h), Triassic Zhifang group (T_2z), and Quaternary (Q). The main mining is no. 5 coal seam of Permian Shanxi Formation. The thickness of the coal seam is between 2.9 m and 9.9 m, with an average thickness of 5.5 m.

2.3. Thermal Hazard Phenomenon. In recent years, the temperature of air flow in underground working face of Bailiang coal mine is above 31°C. The water temperature of the Ordovician limestone aquifer in the floor of the roadway in the north, 508 working face and 502 working face of the mine, reaches 40°C. Xizhuo mine also has a relatively obvious high temperature abnormal phenomenon. The water temperature at the mine water inrush point is also over 37°C in roadway tunneling, and a relatively significant high temperature abnormal phenomenon occurs in both mines.

3. Experiments and Methods

3.1. Temperature Logging Data. The main method to obtain the temperature of underground strata in coalfield exploration is the continuous temperature measurement of borehole fluid system, called temperature logging [41, 42]. Temperature logging data mainly includes two types: approximate steady-state temperature and simple temperature measurement. The approximate steady-state temperature data was generally measured three days after completion, and the drilling fluid and rock temperature have basically reached equilibrium. The measured data can more objectively reflect the real temperature of the stratum. The simple temperature data was usually measured within 1 day after completion, so the temperature data must be corrected before it can be used.

The geothermal data used in this study mainly come from the temperature measurement data of geological exploration holes in the study area. There are 51 boreholes for temperature measurement, including 4 tests of approximate steady-state temperature and 47 tests of simple temperature measurement. On the plane, all temperature measuring holes are evenly distributed in Xizhuo and Bailiang mine, which is well representative (Figure 1).

3.2. Underground Temperature Measurement. Surface drilling is affected by the mining activities and the changes of surface and underground hydrogeological conditions. In order to precisely understand the variation law of ground temperature, this study also compared the previous ground temperature data and measured the temperature of the surrounding rock of coal seam and the outlet point of coal seam floor in Bailiang coal mine.

Underground temperature measurement adopted shallow hole temperature measurement method. This method

Table 2: Temperature measurement results in Bailiang coal mine.

Measuring point	Position	Temperature of measuring point/°C
1	516 working face left side of roadway, no. 5 coal seam	34.8
2	516 working face right side of roadway, no. 5 coal seam	36.2
3	Outlet point of 505 working face	39.2
4	The rock of 505 working face	33.7
5	50 m total ventilation roadway, no. 5 coal seam	34.3
6	100 m total ventilation roadway, no. 5 coal seam	43.3
7	300 m total ventilation roadway, no. 5 coal seam	32.4
8	Wellbore inspection hole, gushing water	40
9	Bu 3-2 poor sealing borehole, gushing water	41
10	518 working face, water gushing point	42
11	518 working face, roadway rock	40.1
12	Ordovician limestone hydrological observation hole, water temperature	40

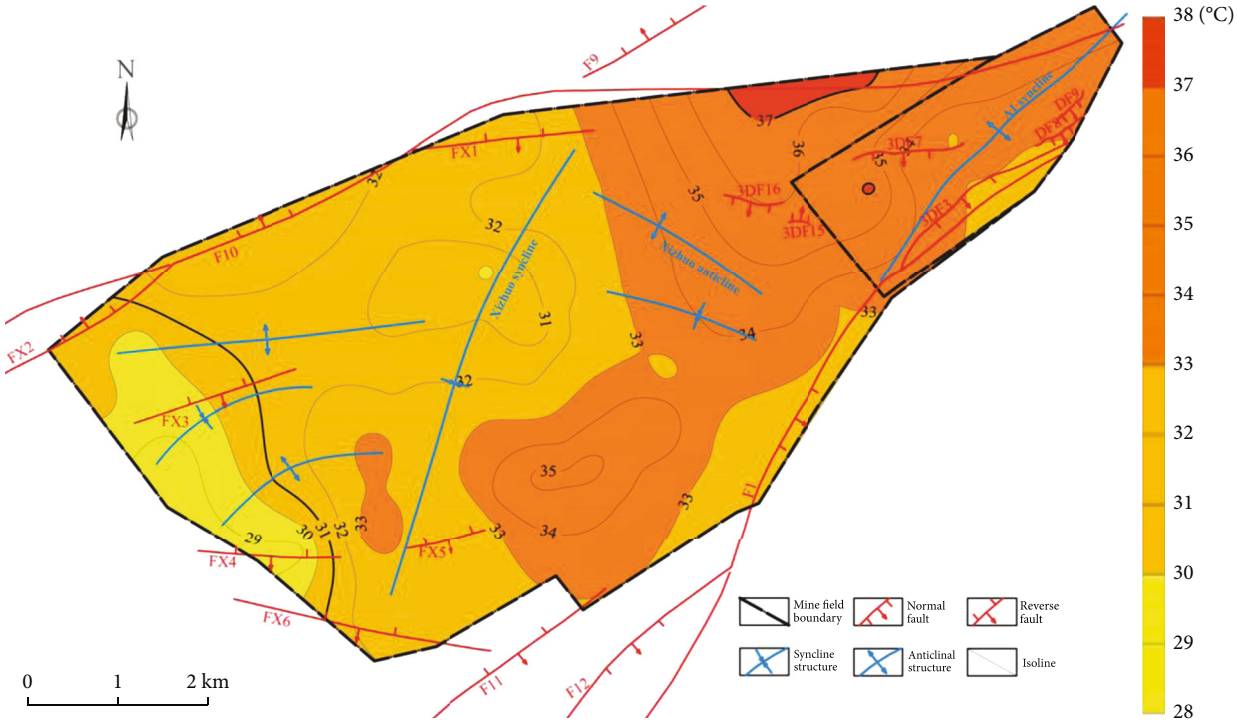

Figure 4: Ground temperature contour map of no. 5 coal seam.

used the pneumatic drill bolt construction technology to drill into the surrounding rock at the target point. Two drilling holes with an included angle ≥45° and a depth ≥2 m at each position were grouped together, and the temperature was measured at the same time (Figure 2). After the drilling was completed, the thermometer was sent to the bottom of the hole through the casing, and the hole top was blocked. The temperature measuring was read every 10 minutes. Stopping the temperature measurement after the thermometer data was stable. The temperature measurement time was generally between 90 minutes and 120 minutes. The temperature measuring instrument used in underground work was composed of a temperature sensor probe and a temperature display, which can be applied to conditions above 100°C. The display device was an AD display device, which adopt COMS micropower inheritance circuit and wide-temperature large-field wide-screen LCD display. The characteristics of AD display device was waterproof, explosion-proof, and seismic (Figure 2).

3.3. Rock Thermal Conductivity Test. Rock thermal conductivity refers to the characteristics of heat transfer of rock, which is the main thermal parameter of rock and the basic data to obtain terrestrial heat flow [43]. The test samples in

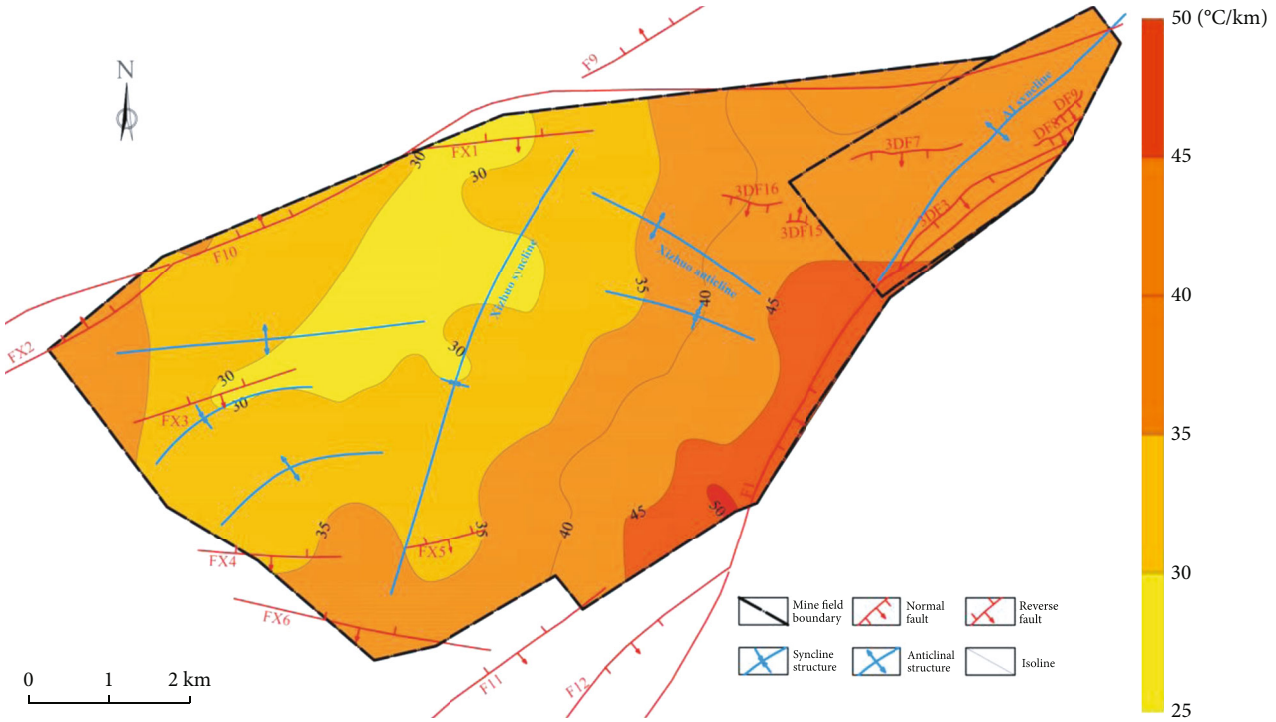

Figure 5: Contour map of geothermal gradient.

this study were collected from two surface supplement exploration holes XC1 and XC2 in Xizhuo mine. Twenty-five representative samples were tested, and the depth range of the samples ranged from 120 m to 600 m. The strata from old to new were involved, basically representing the main rock types of coal measure strata in Weibei coalfield.

3.4. Calculation of Geothermal Gradient. Because the approximate steady-state temperature measurement results are high accuracy, the ground temperature gradient can be calculated and obtained directly by the following formula.

$$T = G(H - H_0) + T_0, \tag{1}$$

where G is the average ground temperature gradient of temperature measuring borehole, ˚C/km; T is the bottom hole temperature, ˚C; T_0 is the temperature of constant temperature zone, ˚C; H is the bottom hole depth, m; H_0 is the depth of constant temperature zone, m. H_0 in the area is 30 m, and T_0 is 16.8˚C.

When using the simple temperature measurement data, the borehole bottom hole temperature (BHT, the same below) must be corrected. In this paper, the Waples and Ramly [44, 45] method was used to correct the bottom hole temperature. This method holds that for BHT data with depth less than 3000 m, the following correction formula was used for prediction:

$$T_c = T_s + f(T_m - T_s), \tag{2}$$

where T_C is the correction temperature within a certain depth at the bottom of the well, ˚C; T_S is the ground temperature corresponding to the correction point, ˚C; f is the correction factor; T_m is the BHT data obtained during temperature measurement, ˚C.

f is given by the following formula:

$$f = \frac{(-0.1462 \ln (\mathrm{TSC}) + 1.699)}{(0.572Z^{0.075})}, \tag{3}$$

where f is the correction factor; TSC is the drilling stop time, h; Z is the drilling depth of the corresponding test point, m.

3.5. Calculation of Terrestrial Heat Flow. Terrestrial heat flow refers to the heat transmitted from the earth's interior to the surface per unit area of the surface or near surface shallow layer. Numerically, it is equal to the product of rock thermal conductivity and vertical geothermal gradient [46].

$$Q = -k \bullet \left(\frac{\Delta T}{\Delta Z}\right), \tag{4}$$

where Q is the earth heat flow, mW/m^2, k is the thermal conductivity, W/m·K, $\Delta T/\Delta Z$ is the ground temperature gradient, ˚C/km.

In order to make the calculated heat flow value more reliable, this paper selected a representative approximate steady-state temperature measurement borehole and used the least square method to fit the linear relationship between ground temperature and depth, so as to obtain the ground temperature gradient value. The calculation range of ground temperature gradient at the calculation point of heat flow

Table 3: Statistics of regional heat flow value.

Drill hole number	Calculation section range (m)	Geothermal gradient (°C/km)	Lithology proportion/%		Weighted average thermal conductivity (W/(m·°C))	Terrestrial heat flow (mW/m^2)
			Mudstone and sandstone	Fine sandstone		
40-1	136.7-510.16	29	0.65	0.35	2.658	77.087
40-2	118-532.44	33	0.61	0.39	2.669	88.086
41-2	108-492.7	35	0.39	0.61	2.735	95.724
41-3	130.42-423.22	45.8	0.71	0.29	2.641	120.976
42-1	134.43-531.90	30	0.71	0.29	2.641	79.230
42-2	98.13-439.1	30	0.90	0.10	2.586	77.575
42-3	104.28-385.79	48.5	0.68	0.32	2.649	128.489
43-1	107.16-490.10	30	0.71	0.29	2.639	79.173
43-2	70.65-424.38	28	0.62	0.38	2.666	74.659
43-3	109.75-385.70	37	0.81	0.19	2.613	96.688
CH209	77.0-429.50	33.4	0.00	1.00	2.860	95.524
CH210	84-508.8	30	0.07	0.93	2.838	85.128
CH211	119.5-464.8	27.1	0.52	0.48	2.696	73.050
J1-1★	123.1-541.12	27	0.56	0.44	2.683	72.441
J1-2	128.65-510.03	29	0.41	0.59	2.728	79.102
J2-1★	143.41-556.80	30	0.59	0.41	2.674	80.214
J2-2	118-538.22	32	0.53	0.47	2.694	86.203
J2-3	129.5-513.38	35	0.56	0.44	2.683	93.900
J3-1	130.5-552.22	29	0.72	0.28	2.637	76.468
J3-2	113.45-535.46	30	0.66	0.34	2.654	79.608
J3-3	132.74-519.28	27	0.66	0.34	2.655	71.692
J3-4	116.49-491.17	29.5	0.71	0.29	2.640	77.868
J3-5	136.5-444.89	36	0.82	0.18	2.608	93.890
J4-1	104.8-529.87	27	0.70	0.30	2.642	71.347
J4-2	113.64-491.92	14	0.71	0.29	2.640	69.952
J4-3	119.2-478.15	33	0.51	0.49	2.699	89.060
J4-4	124-446	38	0.89	0.11	2.589	98.366
J4-5	122.12-409.67	39	0.79	0.21	2.619	102.129
J5-1★	109-501.01	35	0.52	0.48	2.694	94.307
J5-2	116.4-492.79	25	0.60	0.40	2.672	66.806
J5-3	107.55-443.95	33	0.52	0.48	2.695	88.941
J5-4	113-403.55	42	0.95	0.05	2.574	108.089
J5-5	106-371.04	38	0.80	0.20	2.615	99.368
J6-1	99.5-482.75	37	0.71	0.29	2.641	97.718
J6-2	115.9-460.72	34	0.61	0.39	2.670	90.771
J6-3	108.4-410.85	41	0.69	0.31	2.646	108.472
J6-4	124-388.77	35	0.62	0.38	2.666	93.326
J7-1	110.95-455.35	40	0.59	0.41	2.674	106.960
J7-2	101.22-435.2	44	0.69	0.31	2.646	116.444
J7-3	113.5-390.52	34	0.80	0.20	2.615	88.915
J8-1	91-529.94	37	0.58	0.42	2.679	99.115
J8-2	99-326.26	47	0.60	0.40	2.671	125.550
J9-1★	84-502.64	35	0.61	0.39	2.670	93.462
XC1	120.3-541.7	32.9	0.58	0.42	2.677	88.090
XC2	120.08-417.58	42.8	0.70	0.30	2.644	113.175

Note: ★ is stable temperature hole.

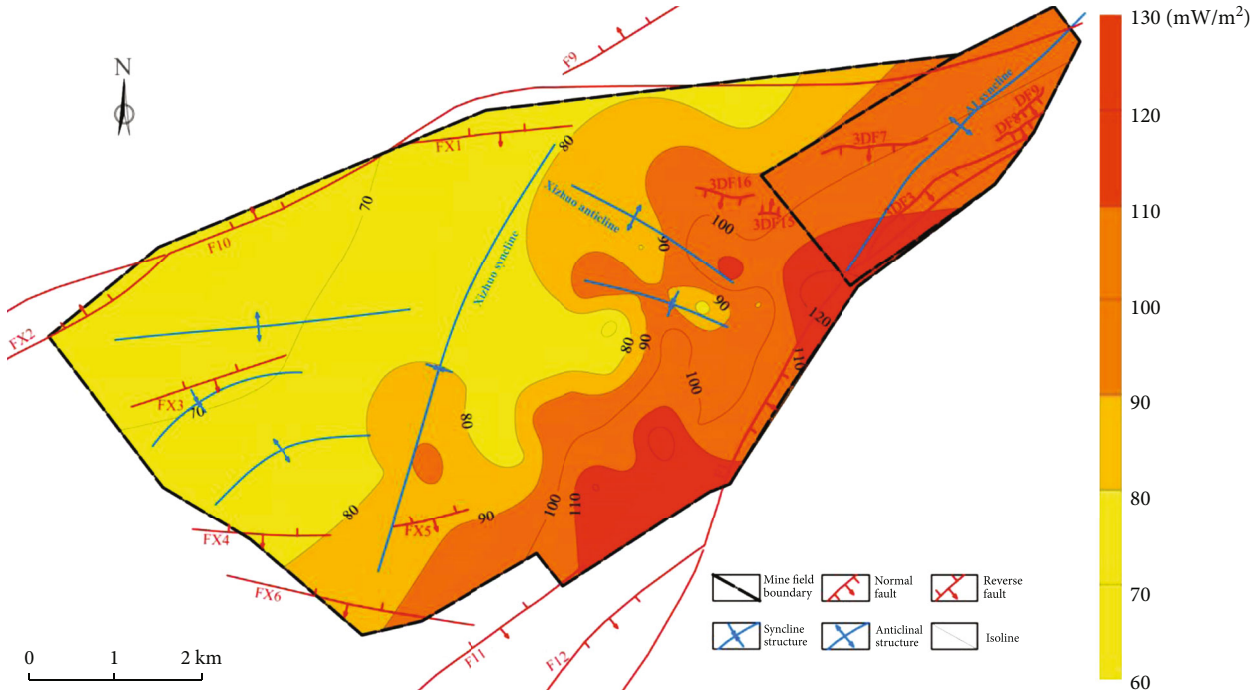

Figure 6: Distribution map of terrestrial heat flow.

Table 4: Statistics of geothermal gradient of stratum.

Stratum	Noncoal strata (°C/km)	Coal-bearing strata (°C/km)	No. 5 coal seam/km (°C/km)	Ordovician strata (°C/km)
Gradient ranges	14~4805	14~82.5	21~101	15~88
Average	31.1	42	54.2	39.7

value is below the bedrock surface. According to the requirements of obtaining heat flow value, well temperature logging and rock thermal conductivity test should be the same borehole, but it is difficult to do in practical work. Considering that the sampling depth of rock samples of Permian coal measure strata is evenly distributed and has sufficient representativeness, the difference of rock thermal conductivity of the same horizon in the study area is small. This paper calculated the average thermal conductivity of each temperature measuring hole by using the "weighted average method" of various lithologic thicknesses of boreholes [47, 48].

4. Results and Discussion

4.1. Current Geothermal Field Distribution Characteristics. According to the test results, the characteristics of the geothermal field in this area were analyzed from the vertical and plane aspects, respectively.

4.1.1. Vertical Distribution. The last test data in the approximate steady-state temperature measurement can basically represent the distribution of the original vertical ground temperature [49]. Therefore, according to the approximate steady-state hole temperature measurement curve in the study area (Figure 3), the vertical ground temperature in this area increases with the increase of depth and shows a good linear relationship.

The results of the rock thermal conductivity in the study area range from 1.95 W/m·°C to 5.07 W/m·°C, with an average value of 3.32 W/m·°C, and the mosts are distributed between 2.5 W/m·°C and 3 W/m·°C (Table 1).

4.1.2. Plane Distribution

(1) Ground Temperature Distribution of No. 5 Coal Seam. The no. 5 coal seam is the main coal seam at present. The thickness of the coal seam is 2.2 m ~7.7 m, with an average of 4.6 m. The underground temperature measurement of Bailiang coal mine is shown in Table 2, and the temperature degree is between 32.4°C and 43.3°C. Combined with borehole temperature data, the coal seam temperature of the whole study area is in the range of 28.5°C ~39.2°C, with an average of 33.13°C, and the most of them are distributed in the range of 32~35°C.

It can be seen from Figure 4 that the ground temperature generally shows the trend of gradual increase from SW to EN. The results indicate that compared with the overlying noncoal stratum, the no. 5 coal seam has a large range of relatively high temperature area. Almost the whole area is a first-class heat hazard area (>31°C), and the northeast is a second-class heat hazard area (>37°C).

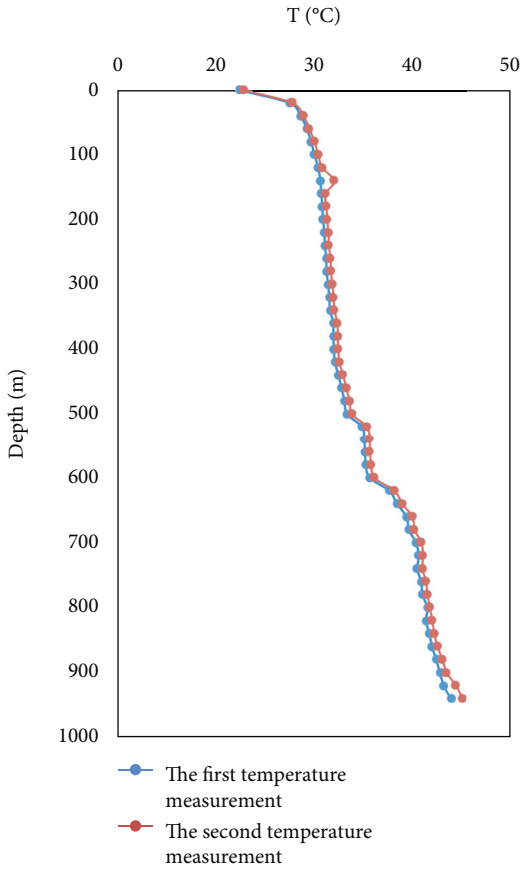

Figure 7: Temperature profile of CH176 borehole.

(2) Geothermal Gradient Distribution. The geothermal gradient in this area is between 25.7°C/km and 54.3°C/km, with an average of 36.6°C/km, and the most of them are 30°C/km~40°C/km. The area with geothermal gradient greater than 30°C/km accounts for 88.31% of the total study area, and the high geothermal is prominent. The regular distribution of geothermal gradient is obvious. The overall performance is the trend of gradually increasing from northwest to southeast, in which the gradient value of F_1 fault zone in the southeast is the highest. And the northwest flank of Xizhuo syncline in the middle and north is the lowest (Figure 5).

4.1.3. Regional Heat Flow Distribution. The heat flow of study area ranges from 66.81 mW/m^2 to 128.49 mW/m^2, with an average of 90.96 mW/m^2 (Table 3 and Figure 6). This is 17.21 mW/m^2 higher than the average heat flow of Hancheng mining area [50], which belongs to an obvious high heat flow area. The distribution law of heat flow value in this area is also obvious, which gradually increases from northwest to southeast. The distribution characteristics is relatively low in northwest, medium in central and high in southeast, and showing an obvious high anomaly area near the proved large fault.

4.2. Main Control Factors of Geothermal Field

4.2.1. Fault Structure. The F_1 fault on the southeast boundary and F_{10} fault on the northern boundary are the main coal controlling structures in the study area. It can be clearly seen from Figures 4 and 6 that there are obvious high-temperature anomalies at the intersection of F_1, F_{10} fault zone, and two major fault zones. The two major faults are tensile normal faults with large drop, long extension, and high angle. This type of fault zone is the main channel for conducting deep underground hot water, resulting in the continuous transmission of deep heat flow to the upper part, changing the original heat flow state [51], and forming the current high heat flow area. The high temperature Ordovician limestone water emitted from the underground coal seam floor near the F_1 fault in Bailiang coal mine also provides evidence for the geothermal control function of the water flowing fault.

4.2.2. Fold Structure. In the A_1 anticline and Xizhuo anticline, the geothermal gradient and terrestrial heat flow showed a decreasing trend from the axis of the anticline to the two flank. At the intersection of A_1 anticline and Xizhuo anticline, the geothermal gradient is above 45°C/km, and the heat flow value is also as high as 120 mW/m^2. On the contrary, the geothermal gradient near the axis of Xizhuo syncline is much lower than that in the anticline area. This feature is mainly due to the lateral difference of rock thermal conductivity, resulting in the enrichment of deep heat flow in the basement uplift area, forming a heat accumulation effect, and the overlying sedimentary cover with low thermal conductivity plays a good role in preserving the heat flow [52]. Hence, the control of basement fluctuation and fold structure on heat flow transmission is also prominent in the study area.

4.2.3. Thermal Conductivity of Coal-Rocks. The thermal conductivity of various rocks in the study area is a wide range. The sandstone is the highest thermal conductivity, followed by mudstone, and coal is the lowest thermal conductivity values. The overall thermal conductivity of all rocks increases with the increase of burial depth and stratigraphic. The thermal conductivity has a certain influence on the distribution of the geothermal field in the vertical direction, and the lower the thermal conductivity of the rocks, the larger the geothermal gradient. The no. 5 coal seam has the smallest thermal conductivity and the largest geothermal gradient. The geothermal gradient of the coal seam is also larger than that of the noncoal seam (Table 4), which also reflects the influence of thermal conductivity on the geothermal gradient.

4.2.4. Influence of Groundwater Activities. The main source of groundwater recharge in the study area is underground runoff outside the area, which flows from NW to SE in the direction and is discharged outside the area through runoff. Due to the influence of geological structure, there are drainage springs distributed in the SE boundary of the study area and F_1 intersection zone. According to the water quality analysis of Xizhuo mine, it is known that the groundwater is highly mineralized and strongly alkaline. The hydrogeochemical environment is a reducing environment, which indicates that the runoff conditions are poor. From the well temperature curve, it is found that most of the northern and northwestern areas of the study area exhibit a linear type,

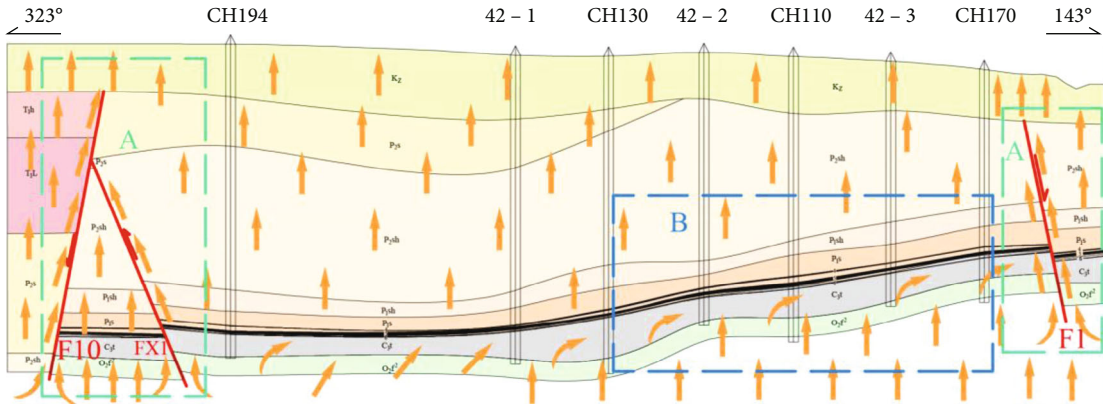

Figure 8: Schematic diagram of the temperature control mode in the study area (1-1′ profile line in Figure 1). The arrow in the figure indicates the direction of heat flow; A is the fault-deep circulation hot water conduction type temperature control mode; B is the heat resistance—folding temperature control mode.

showing the characteristics of good runoff conditions, while the central-eastern area exhibits an upward convex type (Figure 7), especially in the boundary zone along the direction of the F_1 fault is obvious, indicating the influence of lateral high temperature hot water runoff. It is highly consistent with the pattern of the geothermal gradient, i.e., groundwater activities also have an important influence on the distribution of the geothermal field in the study area.

4.3. Forming Mode of Geothermal Field. According to the above analysis, the main controlling factors of the geothermal field in the study area are fault, folding, rock thermal conductivity, and groundwater. The geothermal anomaly temperature control mode in the study area is divided into two categories, which are fault-deep circulation hot water conduction type temperature control mode and coal seam heat resistance-folding type temperature control mode (Figure 8).

(1) *Fault-Deep Circulation Hot Water Conduction Type Temperature Control Model.* After the formation of the coal basin in Chenghe mine area, along with the transformation of relatively strong tectonic movement, two large fault F_1 and F_{10} form horst structural style under the action of stress. First of all, when the fault zone channel is less filled with material or the fracture is more developed, the fault zone itself can form a stable and penetrating heat-conducting channel, gathering a large amount of heat flow upward along the channel. When the temperature is higher than the surrounding environment, the heat will be transferred to the horizontal direction, resulting in the increase of heat flow density in a certain range around the channel. The temperature of the surrounding rock is raised, resulting in the formation of local geothermal anomalies. Second, the existence of water-conducting faults will form a good discharge channel for deep groundwater, and the deep circulating hot water from the deep basement will be discharged to the surface along the discharge channel. The local water circulation will also be generated in the fault zone, which will promote the expansion of heat exchange range and form the geothermal anomaly zone

(2) *Coal Seam Heat Resistance-Fold Type Temperature Control Mode.* The heat flow is easily concentrated in the basement uplift area or the back-slope tectonic axis, with high geothermal temperature, geothermal gradient, and heat flow value. This feature is mainly due to the lateral difference of rock thermal conductivity, which causes the deep heat flow to be enriched in the basement uplift area and forms the heat gathering effect. In addition, influenced by the low thermal conductivity of coal seam, the heat blocking effect is obvious, and the spatial spreading pattern of coal seam is influenced by the folded structure, most of the heat flow occurs horizontally along the layer, which plays the role of heat blocking and flow guiding, resulting in the ground temperature of coal seam and its lower area is obviously higher than that of upper strata

5. Conclusions

(1) The geothermal hazard is obvious in Chenghe mining area, almost the whole area of the main mining no. 5 coal seam in the eastern part of the Chenghe mine area belongs to the first-class heat hazard zone (>31°C), and the northeastern part is the second-class heat hazard zone (>37°C)

(2) The present geothermal gradient ranges from 25.7°C/km to 54.3°C/km, and the geothermal heat flow value varies from 66.81 mW/m^2 to 128.49 mW/m^2. The distribution pattern of geothermal gradient and geothermal heat flow value shows a gradual increase from northwest to southeast, and it is especially prominent near the large fault zone

(3) The main controlling factors of geothermal anomaly are fault, fold, coal-rock thermal conductivity, and groundwater activity in the region. According to

the distribution characteristics of heat flow and the action mechanism of main controlling factors, the geothermal anomaly in the study area is finally divided into two forming modes, i.e. fault-deep circulating hot water uplifting type and coal seam heat resistance-fold type

Data Availability

All data, models, and code generated or used during the study appear in the paper.

Conflicts of Interest

The authors declare no potential conflicts of interest with respect to the research, authorship, and publication of this paper.

Acknowledgments

We thank the China Coal Xi'an Design Engineering Co., Ltd., Shaanxi Coal Chenghe Mining Co., Ltd., and Shaanxi 139 Coal Geology & Hydrogeology Co., Ltd. for providing geological data and samples collection. This work was supported by National Natural Science Foundation of China (Grant no. 41902175), the Shanxi Province Science and Technology Major Special Funding Project (Grant no. 20201101002), the Shaanxi Province Natural Science Basic Research Program Funding Project (Grant no. 2019JQ-245), and the Projects Funded by China Postdoctoral Science Foundation (Grant no. 2019M653873XB).

References

[1] J. W. Lund and A. N. Toth, "Direct utilization of geothermal energy 2020 worldwide review," *Geothermics*, vol. 90, article 101915, 2021.

[2] D. Moya, D. Aldás, and P. Kaparaju, "Geothermal energy: power plant technology and direct heat applications," *Renewable and Sustainable Energy Reviews*, vol. 94, pp. 889–901, 2018.

[3] W. Guowen and K. Jian, "Genetic analysis of geothermal resources in deep-seated fault area in Tonghe County, Northeast China and implications of geothermal exploration," *Sustainability*, vol. 14, no. 9, p. 5431, 2022.

[4] X. Heping, Z. Hongwei, X. Dongjie, H. Wang, R. Zhang, and F. Gao, "Research and reflection on deep coal mining and ultimate mining depth," *Journal of Coal*, vol. 37, no. 4, pp. 535–542, 2012.

[5] Y. Xue, J. Liu, P. G. Ranjith, Z. Zhang, F. Gao, and S. Wang, "Experimental investigation on the nonlinear characteristics of energy evolution and failure characteristics of coal under different gas pressures," *Bulletin of Engineering Geology and the Environment*, vol. 81, no. 1, p. 38, 2022.

[6] P. Hou, Y. Xue, F. Gao et al., "Effect of liquid nitrogen cooling on mechanical characteristics and fracture morphology of layer coal under Brazilian splitting test," *International Journal of Rock Mechanics and Mining Sciences*, vol. 151, p. 105026, 2022.

[7] X. L. Li, S. J. Chen, S. M. Liu, and Z. H. Li, "AE waveform characteristics of rock mass under uniaxial loading based on Hilbert-Huang transform," *Journal of Central South University*, vol. 28, no. 6, pp. 1843–1856, 2021.

[8] X. L. Li, S. J. Chen, and S. Wang, "Study on in situ stress distribution law of the deep mine taking Linyi Mining area as an example," *Advances in Materials Science and Engineering*, vol. 9, no. 4, Article ID 5594181, 2021.

[9] H. Liu, B. Zhang, X. Li et al., "Research on roof damage mechanism and control technology of gob-side entry retaining under close distance gob," *Engineering Failure Analysis*, vol. 138, no. 5, article 106331, 2022.

[10] Y. Xue, J. Liu, P. G. Ranjith, F. Gao, H. Xie, and J. Wang, "Changes in microstructure and mechanical properties of low-permeability coal induced by pulsating nitrogen fatigue fracturing tests," *Rock Mechanics and Rock Engineering*, vol. 56, 2022.

[11] Y. Xue, J. Liu, P. G. Ranjith, F. Gao, Z. Zhang, and S. Wang, "Experimental investigation of mechanical properties, impact tendency, and brittleness characteristics of coal mass under different gas adsorption pressures," *Geomechanics and Geophysics for Geo-Energy and Geo-Resources*, vol. 8, no. 5, p. 131, 2022.

[12] H. Manchao, "Application of HEMS cooling technology in deep mine heat hazard control," *Mining Science and Technology*, vol. 19, no. 3, pp. 269–275, 2009.

[13] L. He, S. Hu, S. Huang et al., "Heat flow study at the Chinese continental scientific drilling site: borehole temperature, thermal conductivity and radiogenic heat production," *Journal of Geophysical Research*, vol. 113, pp. 4392–4404, 2009.

[14] H. Manchao and X. Min, "Development of HEMS deep well cooling system and countermeasures for heat damage control," *Journal of Rock Mechanics and Engineering*, vol. 27, no. 7, pp. 1353–1361, 2008.

[15] P. Zhonghe, H. Shaopeng, H. Shengbiao, Zhao Ping, and H. Lijuan, "Progress and prospects of geothermal research in China," *Geoscience*, vol. 49, no. 3, pp. 719–727, 2014.

[16] P. Tao, W. Jiwen, R. Ziqiang, X. Sheng-Ping, and Z. Hai-Chao, "Geodetic heat flow distribution and its tectonic control in the two Huai coal fields," *Journal of Geophysics*, vol. 58, no. 7, pp. 2391–2401, 2015.

[17] X. Shengping, P. Tao, W. Jiwen, Z. Haichao, and R. Ziqiang, "Characteristics of thermal conductivity of coal-based rocks in the two Huai coal fields and its influence on the geothermal field," *Journal of Collegiate Geology*, vol. 42, no. 6, pp. 76–81, 2014.

[18] S. Wang, J. Hu, J. Yan et al., "Assessment of geothermal resources in petroliferous basins in China," *Mathematical Geosciences*, vol. 51, no. 3, pp. 271–293, 2019.

[19] S. Shaohua, Z. Qinghua, Z. Jianhua, and L. Shunsheng, "Study of tectonothermal events in the Ordos Basin," *Science Bulletin*, vol. 42, no. 3, pp. 306–309, 1997.

[20] R. Zhanli, Z. Sheng, G. Shengli, C. Junping, X. Yuanyuan, and X. Hui, "Tectonothermal evolutionary history of the Ordos Basin and its reservoir-forming and mineralization significance," *Chinese Science D Series*, vol. 37, Suppl. 1, pp. 23–32, 2007.

[21] R. Zhanli, Y. Qiang, C. Junping et al., "Thermal evolutionary history of the Ordos Basin and its role in controlling hydrocarbons," *Geological Foreground*, vol. 24, no. 3, pp. 137–148, 2017.

[22] C. Zhanpeng, R. Zhanli, X. Ping, Q. Kai, and C. Zhanjun, "Recovery of Ordovician thermal evolutionary history and

hydrocarbon generation history in the southwest margin of the Weibei uplift in the Ordos Basin-example of the Lingyou Xunyi area," *Journal of Geology*, vol. 90, no. 3, pp. 513–520, 2016.

[23] Z. Yang, M. Genxu, Z. Hui, W. Ke, and Z. Yage, "Geothermal field delineation in the Guanzhong Basin and its geological influences," *Geology of China*, vol. 44, no. 5, pp. 1017–1026, 2017.

[24] W. Zhao, Q. Dong, Z. Chen et al., "Weighted information models for the quantitative prediction and evaluation of the geothermal anomaly area in the plateau: a case study of the Sichuan-Tibet railway," *Remote Sensing*, vol. 13, no. 9, p. 1606, 2021.

[25] S. Liu, C. Ye, Q. Sun et al., "Detection of geothermal anomaly areas with spatio-temporal analysis using multitemporal remote sensing data," *IEEE Journal of Selected Topics in Applied Earth Observations and Remote Sensing*, vol. 14, pp. 4866–4878, 2021.

[26] Y. Yina and M. Zhaoping, "Geothermal distribution characteristics in the Qinshui Basin and its significance to the production of coalbed methane," *ACS Omega*, vol. 6, pp. 18914–18927, 2021.

[27] I. Panea and V. Mocanu, "Geophysical analysis of major geothermal anomalies in Romania," *Pure and Applied Geophysics*, vol. 174, no. 11, pp. 4153–4169, 2017.

[28] S. Weiye, W. Yun, L. Qilin, and F. Shaohui, "A study on hydrogeochemistry and tectonic activity features of hot springs in the Red River fault zone," *Bulletin of Mineralogy, Petrology and Geochemistry*, vol. 41, pp. 612–624, 2022.

[29] L. Qiongying and H. Lijuan, "Tectono-thermal modeling of the Bohai Basin since the Cenozoic," *Chinese Journal of Geophysics*, vol. 62, no. 1, pp. 219–235, 2019.

[30] H. Shaolong, "Analysis of ground temperature distribution pattern and its factors in Liu Zhuang well field," *Mining Safety and Environmental Protection*, vol. 31, no. 5, pp. 26–28, 2004.

[31] P. Tao, R. Ziqiang, W. Jiwen, and Z. Hongmei, "Characteristics of the present-day geothermal field and its tectonic control in the deep Panji mining area," *Journal of Collegiate Geology*, vol. 23, no. 1, pp. 157–164, 2017.

[32] Z. Jian, F. Gui, and H. Yubei, *The Deep High Temperature Characteristics and Geodynamic Background of Geothermal Anomaly Areas in Eastern China*Earth Science Frontiers.

[33] E. Jolie, S. Scott, J. Faulds et al., "Geological controls on geothermal resources for power generation," *Nat Rev Earth Environ*, vol. 2, no. 5, pp. 324–339, 2021.

[34] T. Uzelli, M. F. Şener, İ. Dölek, A. Baba, H. Sözbilir, and R. K. Dirik, "Structural controls and hydrogeochemical properties of geothermal fields in the Vartoregion, East Anatolia," *Turkish Journal of Earth Sciences*, vol. 30, pp. 1076–1095, 2021.

[35] S. Guo, C. Zhu, N. Qiu et al., "Present geothermal characteristics and influencing factors in the Xiong'an New Area, North China," *Energies*, vol. 12, no. 20, p. 3884, 2019.

[36] Z. Y. Fan, S. Q. Xiong, C. C. Yu, G. B. Zhang, X. Y. Zhang, and B. Hu, "Geothermal distribution characteristics and sedimentary basin geothermal system in the severe cold region of Northeast China," *Applied Geophysics*, vol. 17, no. 3, pp. 321–337, 2020.

[37] X. Chenghua, Y. Dandan, and L. Zujiang, "Recharge sources and genetic model of geothermal water in Tangquan, Nanjing, China," *Sustainability*, vol. 13, no. 8, p. 4449, 2021.

[38] K. Duolei, H. Yunqiang, D. Jianghai, S. Dongzhong, X. Heming, and L. Jie, "Study on fire prevention technology during coal face stoping in close-distance coal seam under condition of deep mine and high ground temperature," *Coal Technology*, vol. 41, no. 1, pp. 170–173, 2022.

[39] Z. Jingzhong, L. Qimeng, and J. Qiding, "Geothermal distribution and thermal damage prediction in Xutuan coal mine," *Coal Engineering*, vol. 53, no. 4, pp. 131–135, 2021.

[40] N. Siyun, Z. Yefu, and Z. Chuanjun, "Study on fire prevention under high ground temperature and rock burst in deep mine," *Shandong Coal Science and Technology*, vol. 10, pp. 126-127, 2020.

[41] W. Huayu, L. Shaowen, and L. Xiao, "Present geothermal regime of the Lower Yangtze area, South China," *Journal of China Coal Society*, vol. 38, no. 5, pp. 896–900.

[42] X. Y. Tang, S. P. Huang, S. C. Yang, G. Z. Jiang, and S. B. Hu, "Correcting on logging-derived temperatures of the Pearl River Mouth Basin and characteristics of its present temperature field," *Geophysics*, vol. 59, no. 8, pp. 2911–2921.

[43] G. Pingye, B. Mohua, L. Qingbo, and H. Manchao, "Research progress of accurate measurement and characterization model of effective thermal conductivity of rock," *Chinese Journal of Rock Mechanics and Engineering*, vol. 39, no. 10, pp. 1983–2013, 2020.

[44] D. W. Waples, J. Pacheco, and A. Vera, "A method for correcting log-derived temperatures in deep wells, calibrated in the Gulf of Mexico," *Petroleum Geoscience*, vol. 10, no. 3, pp. 239–245, 2004.

[45] D. W. Waples and M. Ramly, "A statistical method for correcting log-derived temperatures," *Petroleum Geoscience*, vol. 7, no. 3, pp. 231–240, 2001.

[46] Z. Kaizhen, P. Yumao, C. Yan et al., "Heat flow of the Yingdong area in Qaidam Basin and its influencing factors," *Earth Science*, vol. 42, pp. 1–17, 2004.

[47] H. Zhengguang, L. Chiyang, and Z. Junfeng, "A study on geothermal field and its geological significance in southern area of the North China Craton," *Geological Review*, vol. 55, no. 3, pp. 428–433.

[48] Z. X. Sun, W. Zhang, B. Q. Hu, and T. Y. Pan, "Heat flow and geothermal field in the Qinshui Basin," *Geophysics*, vol. 49, no. 1, pp. 123–128, 2006.

[49] R. Ziqiang, W. Jiwen, Z. Haichao, S. Shuhao, and P. Tao, "Groundwater control of present-day geothermal field in Huainan mine area," *Coal Mine Safety*, vol. 46, no. 7, pp. 193–203.

[50] G. Z. Jiang, P. Gao, S. Rao et al., "Compilation of heat flow data in the continental area of China," *Geophysics*, vol. 59, no. 8, pp. 2892–2910.

[51] K. Beom Jun, W. Sanginn, and Y. Chanyoung, "Effect of heat injection through a vertical drain on clay consolidation," *KSCE Journal of Civil Engineering*, vol. 25, no. 9, pp. 3245–3253, 2021.

[52] Z. Wang, C. Zhang, G. Jiang, J. Hu, X. Tang, and S. Hu, "Present-day geothermal field of Xiongan New Area and its heat source mechanism," *Geophysics*, vol. 62, no. 11, pp. 4313–4322.